A Topology-based Array Compensation Empowered by Equivalent Current Modeling of TM_{10} Patch Antennas for Cross-Polarization Reduction

Taeyeong Yoon[*], **(Graduate Student Member, IEEE), Uichan Park**[*], **(Graduate Student Member, IEEE), Minje Kim**[*], **(Graduate Student Member, IEEE), Sanghun Lee**[*], **(Graduate Student Member, IEEE), Young-Seok Lee**[*], **(Graduate Student Member, IEEE), Sangwook Nam**[*], **(Senior Member, IEEE), AND Jungsuek Oh**[*], **(Senior Member, IEEE)**

[1]the Department of Electrical and Computer Engineering (ECE), Institute of New Media and Communications (INMC), Seoul National University, Seoul 08826, Republic of Korea

CORRESPONDING AUTHOR: Jungsuek Oh (e-mail: jungsuek@snu.ac.kr).

ABSTRACT This paper introduces a comprehensive analysis of cross-polarization effects originating from current imbalances in patch antennas and array configurations. A simplified yet broadly applicable mitigation strategy is proposed, offering a generalized approach to improve cross-polarization performance for antenna arrays operating in the TM_{10} mode. In contrast to earlier works that predominantly employed heuristic array rotation techniques, the present work adopts a systematic modeling approach to elucidate and regulate cross-polarization across a wide range of array scales and topologies. By utilizing electric current modeling at both the single-element and array levels, and analyzing radiation behavior in multiple planes, the beam pattern characteristics are thoroughly examined. Several optimized array configurations, specifically targeting cross-polarization suppression, are proposed. The proposed array system incorporates a series-type power divider, validated through both simulation and measurement, demonstrating significant suppression of cross-polarization over all scan angles. Notably, the fabricated series power divider achieves amplitude and phase mismatches of less than 3 dB and 10 degrees, respectively, across 16 output branches. The analytical and empirical results outlined in this work establish a conceptual design methodology that achieves substantial cross-polarization reduction without altering individual element geometries. Most significantly, a cross-polarization discrimination (XPD) level of -40 dB is attained in beamforming scenarios. These findings confirm that enhanced cross-polarization performance can be systematically realized by refining array sequencing and periodicity.

INDEX TERMS Cross-polarization suppression of patch antennas, current imbalance analysis, array configuration, series power divider.

I. INTRODUCTION

RECENTLY, managing multi-user communication systems efficiently has necessitated the integration of various forms of diversity [1], [2]. To support such functionality, it is critical to consider multiple domains—namely time, frequency, spatial, and polarization diversity [3], [4].
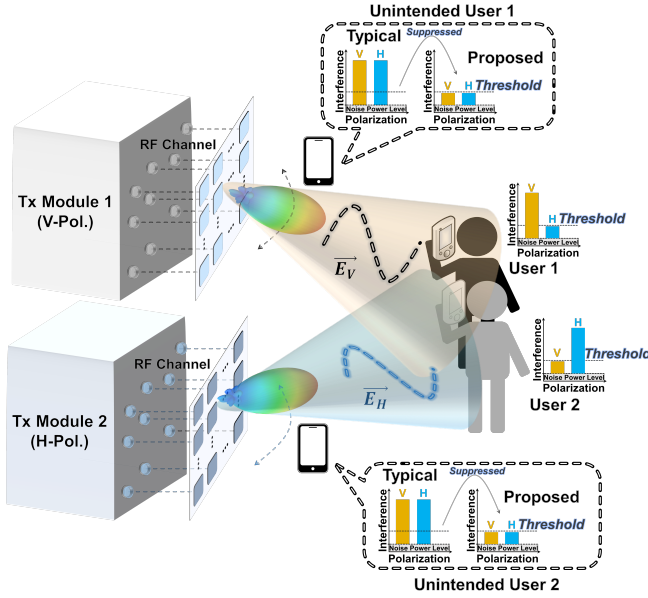
FIGURE 1. Conceptual illustration of polarization diversity applied to a communication system.

Among these, polarization diversity is particularly significant from a wave propagation standpoint, as it plays a central role in mitigating interference within wireless links [5], as illustrated in Fig. 1. While polarization discrimination is typically effective in the main lobe of antenna arrays, interference arising from cross-polarization becomes problematic in undesired angular regions due to the inherent properties of cross- and co-polarized radiation patterns. To address this challenge, this study introduces a systematic approach to suppress cross-polarization interference by modeling the magnetic current distribution in each radiating element and strategically configuring (and phase-inverting) the array, all while preserving the individual antenna design. The issue of polarization diversity becomes even more critical within the industrial, scientific, and medical (ISM) band at 5.8 GHz, where multiple users simultaneously operate within the same spectral band [6]–[9].

Microstrip patch antennas have become a prevalent choice for wireless systems due to their structural simplicity and design convenience. However, when operating in the TM_{10} mode [10], these antennas inherently exhibit cross-polarization owing to geometric asymmetries. To address this, several mitigation techniques have been introduced at the element level, including the use of shorting pins [11]–[15], metallic inclusions [16], parasitic structures [17], and suspended transmission lines [18]. Although effective to some extent, these methods are constrained by the intrinsic limitations of single-element design and lack flexibility in broader array applications. To overcome these limitations, prior works have explored array-level modifications—particularly element rearrangement—to enhance cross-polarization performance [19]–[22]. While these efforts validated the significance of array configuration, they often lacked detailed theoretical analysis and comprehensive modeling, thereby limiting the generalizability of their findings.

This work addresses the above gaps by providing several key contributions:

1) A detailed modeling approach is introduced to analyze cross-polarization mechanisms, focusing on magnetic current imbalances induced by asymmetrical feed structures, and their impact on beam pattern formation.
2) An equivalent electric current representation is formulated, accounting for the electron rotation within the cavity, to better explain the linear polarization behavior determined by the electric field orientation.
3) The proposed model is validated across both element and array levels, and an arrangement methodology is proposed to mitigate cross-polarization across all scan angles through axis-wise configuration strategies.
4) A sidelobe-level reduction technique is developed through periodicity control within the array, supported by analytical evaluation using electric field distributions and array factor formulations.
5) To ensure the practical validity of the proposed approach under beam steering conditions, a hardware implementation is carried out using a beamforming board and custom-designed power divider.

In this work, an electric current modeling approach is established by accounting for magnetic current imbalances arising from structural asymmetries. Rather than relying on physical surface currents on the patch, an equivalent representation based on the rotational behavior of electrons is employed to more clearly interpret polarization characteristics. This modeling enables a deeper understanding of the mechanisms leading to cross-polarization degradation, with the analysis extended to the array level in Section II. In Section III, experimental validation is conducted using a beamforming system, where signal power is distributed via a line-based series power divider optimized for structural compactness. Compared to conventional parallel Wilkinson divider topologies, the proposed solution offers notable miniaturization. A beamforming-capable circuit board is also designed and verified, confirming that the proposed method achieves substantial cross-polarization suppression across all steering directions.

II. Cross-Polarization Analysis of Patch Antennas
A. Single-Element Evaluation
Fig. 2(a) presents a three-dimensional depiction of a microstrip patch antenna excited in the TM_{10} mode, highlighting the orientation of the electric field corresponding to linear polarization. When this excitation is interpreted using a cavity-based framework, the mode can be equivalently represented as a magnetic current distribution, as illustrated in Fig. 2(b). In this representation, the currents labeled $M_{C,1}$ and $M_{C,2}$ are associated with co-polarized radiation,
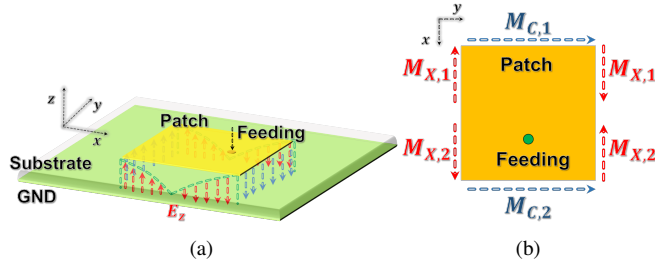
FIGURE 2. Illustration of patch antennas operating in the TM_{10} mode: (a) three-dimensional structural model and (b) corresponding magnetic current distribution.
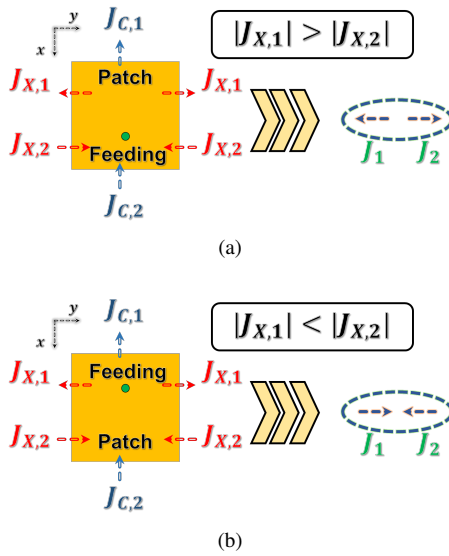

FIGURE 3. Illustrations of patch antennas operating in the TM_{10} mode and the resulting imbalance: (a) equivalent electric current distribution and (b) excitation model with out-of-phase behavior.
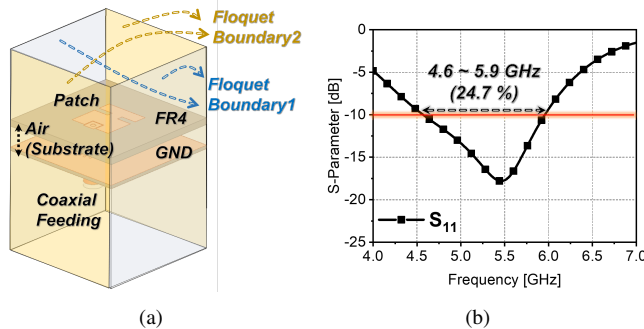

FIGURE 4. (a) Simulation setup used for array antenna design and (b) simulated *S*-parameter results.

whereas $M_{X,1}$ and $M_{X,2}$ are responsible for generating cross-polarization components. To reconcile the behavior of magnetic and electric currents, the model incorporates the rotational dynamics of electron movement, as shown in Fig. 3(a).

Importantly, probe-fed patch antennas inherently exhibit structural asymmetry along the y-axis, which leads to an imbalance between $J_{X,1}$ and $J_{X,2}$. This asymmetry gives
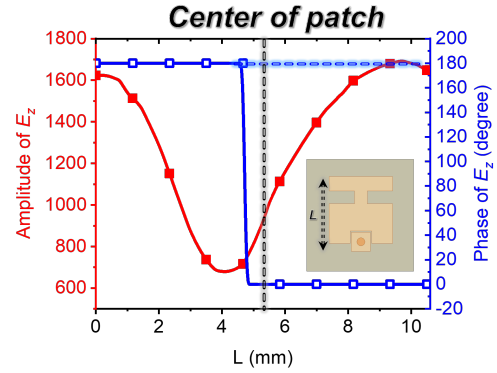

FIGURE 5. The extracted electric field distributions (E_z in Fig. 2(a)) of both magnitude and phase at the left side edge of the patch.
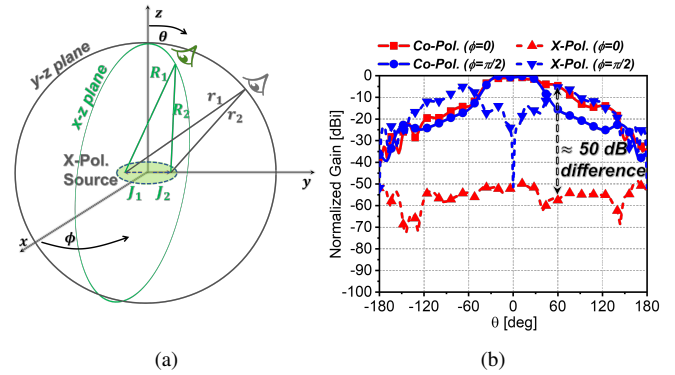

FIGURE 6. (a) Electric current modeling of cross-polarization sources and (b) corresponding simulated beam pattern of the proposed antenna at 5.8 GHz.

rise to undesirable cross-polarized radiation. To analytically capture this effect, the cross-polarization sources—denoted as J_1 and J_2—are modeled in Fig. 3(a) and (b), each corresponding to different feed positions while preserving co-polarization integrity. Notably, the condition depicted in Fig. 3(b) requires a phase excitation offset of 180° relative to Fig. 3(a). The resulting cross-polarization source within a single patch can be interpreted as a dipole comprising out-of-phase current components.

To validate the proposed modeling framework, a single-element antenna was designed and simulated using Floquet boundary conditions in ANSYS HFSS, as depicted in Fig. 4(a). The antenna structure employs a dual-layer configuration composed of thin FR-4 substrates for copper deposition, while air is introduced as an interstitial dielectric to improve the bandwidth of the indirect feeding mechanism [23]–[25]. The simulated performance, shown in Fig. 4(b), confirms an operational bandwidth ranging from 4.6 to 5.9 GHz, corresponding to a fractional bandwidth of 24.7 %.

The simulated distributions of the amplitude and phase of the electric field associated with the TM_{10} mode are presented in Fig. 5, corresponding to the patch-ground region at the edges illustrated in Fig. 2(a). The results clearly exhibit imbalance in both amplitude and phase, deviating from the ideal condition in which the electric field magnitude
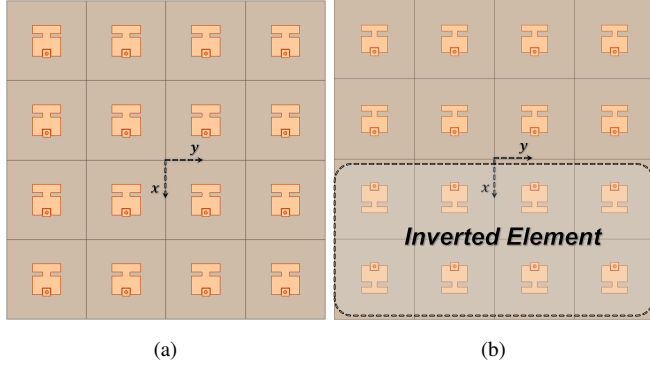
FIGURE 7. Configuration of a 4×4 array: (a) conventional layout and (b) the proposed element arrangement.
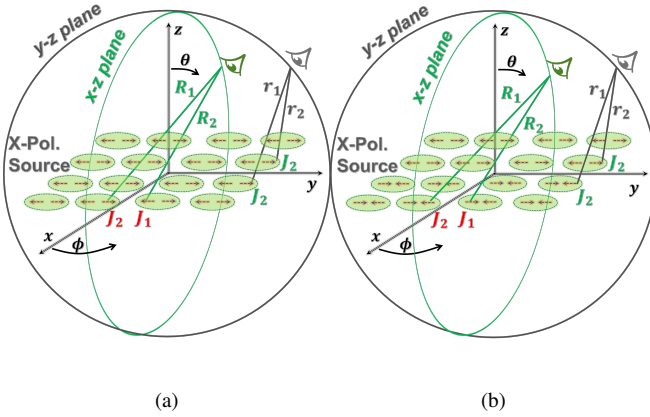

FIGURE 8. Electric current modeling of cross-polarization sources for (a) the conventional array and (b) the proposed array.
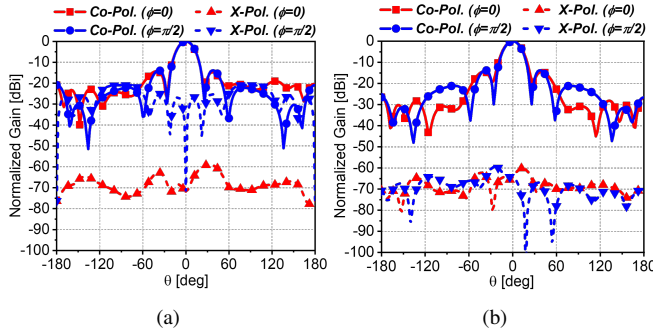

FIGURE 9. Simulated radiation patterns at 5.8 GHz for (a) the conventional array and (b) the proposed array.

is minimized and the phase is reversed at the center of the patch. This imbalance is attributed to structural asymmetry introduced by the feeding mechanism. Unlike conventional approaches that rely on surface current visualization to infer cross-polarization behavior, the present study introduces a field-driven equivalent current modeling approach. Specifically, the electric field components observed at the non-radiating edges of the patch are interpreted in terms of

equivalent magnetic currents. These magnetic currents are then transformed into electric current models by considering the rotational motion of electrons within the cavity. This formulation enables a simplified yet physically meaningful representation of the cross-polarization mechanism, particularly in the context of array design. The issue of imbalance also persists in various feeding schemes, such as aperture-coupled [26], proximity-coupled [27], and direct feeding [28], [29], all of which tend to introduce structural asymmetries during implementation. Consequently, these configurations frequently fail to maintain uniformly low cross-polarization levels across the angular spectrum.

To investigate the radiation behavior arising from a single cross-polarization source, a dedicated model was developed, as shown in Fig. 6(a). The green and gray planes represent the x-z and y-z planes, respectively, (i.e., $\phi = 0$ and $\phi = \pi/2$). In this configuration, the far-field distances from the two out-of-phase currents aligned along the y-axis are analyzed as single cross-polarization source in Fig. 6(a). For R_1 and R_2, the distances remain symmetric with respect to all θ, leading to complete cancellation. In contrast, r_1 and r_2 show angular dependency, resulting in unequal path lengths except at $\theta = 0°$. As a result, the considerable cross-polarization components emerge in the far-field, as depicted in Fig. 6(b).

B. Array Analysis

To mitigate cross-polarization in the y-z plane while preserving the radiation characteristics in the x-z plane, optimization was performed prior to array integration. The 4×4 array configurations are illustrated in Fig. 7(a) and (b), representing the conventional and proposed layouts, respectively. It is important to note that, in the proposed configuration, a $180°$ phase shift is applied to the inverted elements to retain the intended co-polarization properties. This phase inversion causes the cross-polarized currents to be directed oppositely, facilitating their cancellation through appropriate spatial arrangement.

To analyze the far-field behavior of the cross-polarized array, Fig. 8(a) and (b) examine current distances in the x-z and y-z planes. Similar to the single-element case, the x-axis symmetric currents (R_1, R_2) consistently maintain equal path lengths across all θ. While r_1 and r_2 also match under certain array conditions, they differ in behavior compared to the single-element configuration. However, in the proposed array design featuring inverted elements, all distances—R_1, R_2, r_1, and r_2—are made symmetrical. As a result, in the y-z plane, opposing currents at equal distances effectively cancel each other, thereby suppressing cross-polarization.

The radiation patterns at 5.8 GHz for the conventional and optimized arrays are presented in Fig. 9(a) and (b), respectively. The proposed configuration achieves superior cross-polarization suppression in all angular directions, without modifying the elemental antenna structure. Notably, implementing this approach requires a $180°$ relative phase delay,
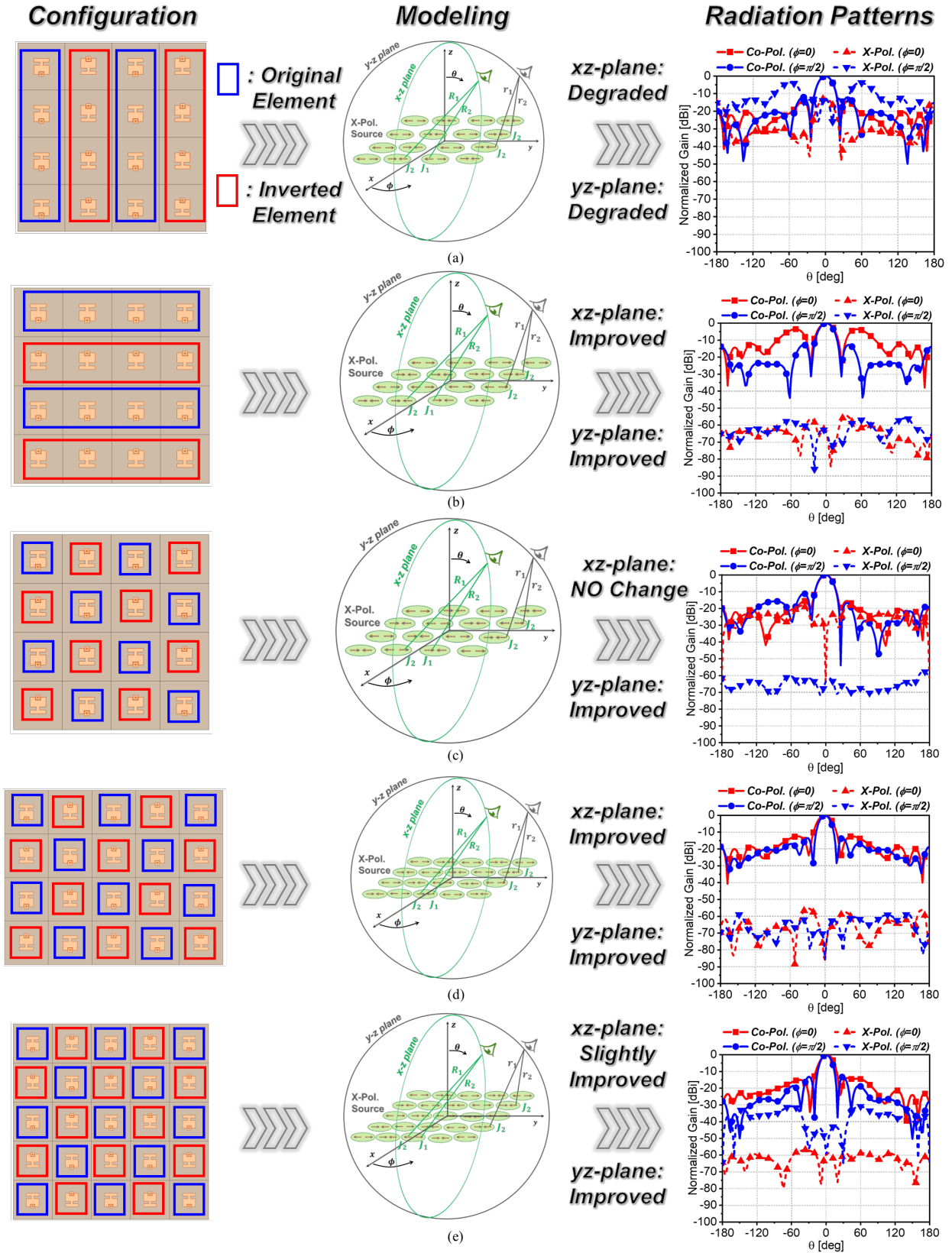
FIGURE 10. Radiation pattern results for various configurations derived from current modeling: (a) flipped along the y-axis, (b) flipped along the x-axis, (c) flipped along both axes, (d) flipped along both axes with an odd-numbered array in the y-direction, and (e) symmetric configuration with both-axis flipping.
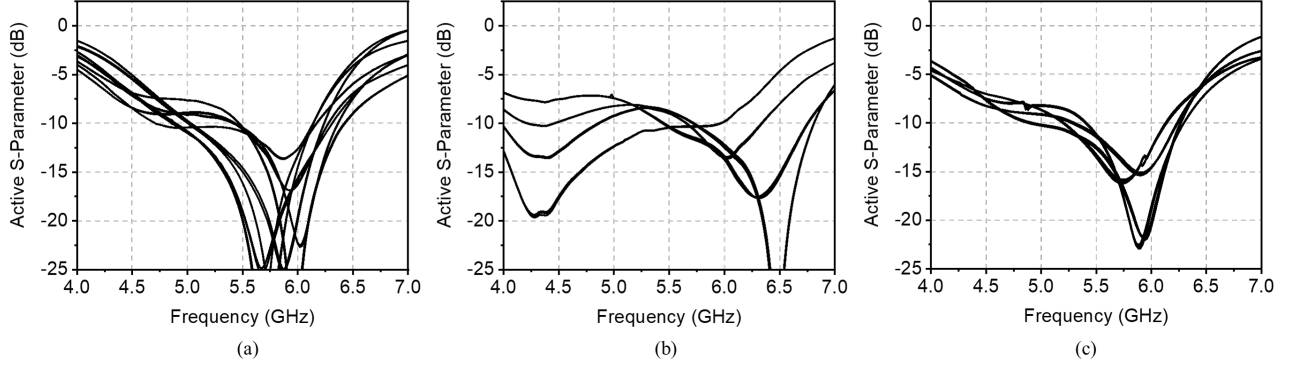
FIGURE 11. Active *S*-parameter results for (a) the conventional array, (b) the configuration in Fig. 10(b), and (c) the proposed array layout.
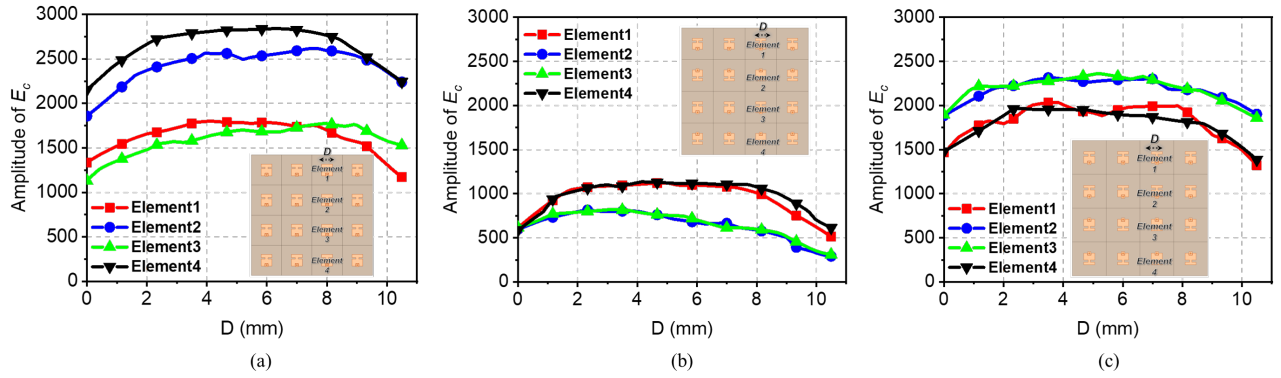

FIGURE 12. Electric field distributions at the radiating edge for (a) the conventional array, (b) the configuration in Fig. 10(b), and (c) the proposed array.
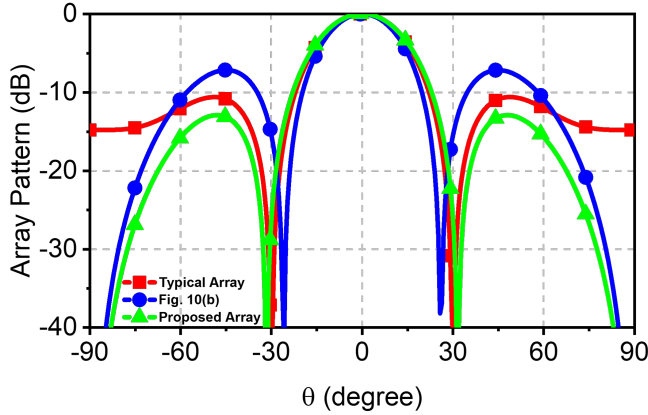

FIGURE 13. Computed array radiation patterns for (a) the conventional arrangement, (b) the configuration shown in Fig. 10(b), and (c) the proposed array configuration.

which in this study was realized through a custom-designed beamforming board to facilitate experimental validation.

C. Enlarging The Analysis to The Array

Fig. 10(a) through (e) present a series of modeling cases in which the array arrangement and the number of elements are systematically varied, along with the corresponding simulation results. These cases demonstrate that not only the cross-polarization characteristics but also the co-polarization performance (e.g., side lobe level) are significantly influenced by the array configuration and arrangement. To effectively visualize the array configuration, blue and red boxes are used to represent the original and inverted elements, respectively. These elements are excited with a 180° phase difference. This modeling strategy is based on equivalent electric current representations extracted from edge electric fields, as previously discussed in Section II. In Fig. 10(a), the array is alternated along the y-axis, resulting in in-phase current distributions in both the x-z and y-z planes. As a result, this leads to a degradation in cross-polarization suppression across all θ, since the energy from the cross-polarization source will be added. Fig. 10(b) illustrates the result of alternating elements along the x-axis, a method also adopted in [19]. This configuration yields improved cross-polarization performance in both the x-z and y-z planes due to the introduction of oppositely directed currents across both axes.

Further extension of the concept to a bi-axial alternating configuration is presented in Fig. 10(c). In this case, in-phase currents appear in the x-z plane, while the y-z plane exhibits
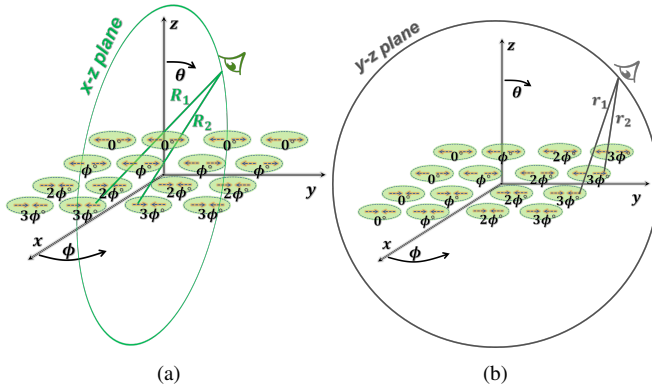
FIGURE 14. Electric current modeling of cross-polarization sources under beamforming scenarios for (a) the x-z plane and (b) the y-z plane.
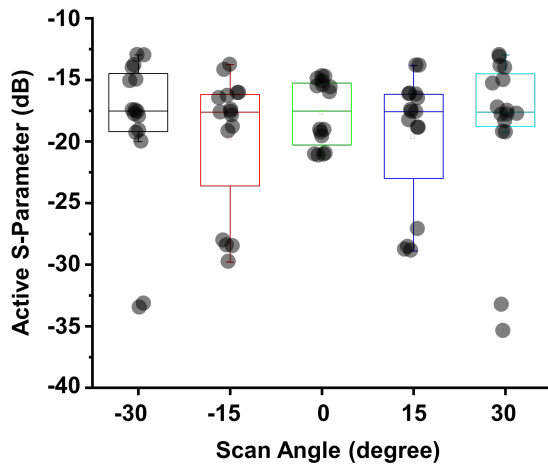

FIGURE 15. The scatter distribution chart of an active *S*-parameter values with respect to scan angle at 5.8 GHz.

FIGURE 16. Flowchart outlining the design methodology for arrays with enhanced cross-polarization suppression.

out-of-phase behavior. As a result, the cross-polarization trend becomes the inverse of that observed in the typical arrangement: the degraded cross-polarziation pattern generated on the xz-plane. Moreover, Fig. 10(d) explores the impact of altering the number of array elements, particularly through the introduction of an odd-number configuration along the y-axis. This adjustment enables the strategic placement of out-of-phase current pairs in the x-z plane, leading to improved cross-polarization characteristics across all angular planes. Lastly, Fig. 10(e) considers the case where both axes consist of an odd number of elements. While the current cancellation condition is preserved along the x-axis, uncancelled current components remain along the y-axis, resulting in a y-z plane performance that surpasses the typical array but remains inferior to the proposed optimal configuration.

The flexibility of the proposed modeling approach allows for the design of a variety of array configurations with enhanced cross-polarization performance. A deeper understanding of the criteria for selecting an optimal configuration can be obtained by examining both the active *S*-parameter responses and the electric field distributions at the patch edge. These results are shown in Fig. 11(a)–(c) and Fig.

12(a)–(c), respectively. Specifically, Fig. 11(a), (b), and (c) correspond to the active *S*-parameter results for the arrays shown in Fig. 7(a), Fig. 10(b), and Fig. 7(b), which represent the typical, intermediate, and proposed array configurations. In all cases, equal magnitude and phase excitation were applied to each port.

Because the typical configuration is modeled to match the conditions used in Floquet-mode simulations, it serves as the baseline reference. Maintaining consistent adjacent element structures is critical for preserving intended antenna characteristics from an array-level perspective. As seen in Fig. 11(b), the array configuration from Fig. 10(b)—which modifies the neighboring element relationships—shows degraded active *S*-parameter performance near 5.8 GHz. However, this degradation is mitigated in the proposed configuration through periodicity control, as demonstrated in Fig. 11(c). Accordingly, it is evident that the desired antenna performance can be retained by adopting the configuration strategies outlined in Fig. 11(a) and (c).

Fig. 12(a), (b), and (c) display the electric field distributions at the radiating edges of four antenna elements arranged along the x-z plane for each array configuration. The co-polarized electric field component is denoted as E_c. Variations in electric field amplitudes across these configurations are reflective of corresponding changes in the active S-parameters. Moreover, particular attention should be given to the field strength within individual array elements. In the typical configuration (Fig. 12(a)), elements 2 and 4 exhibit higher field magnitudes compared to elements 1 and 3. Conversely, in the configuration shown in Fig. 10(b), elements 1 and 4 dominate in amplitude, as illustrated in Fig. 12(b). In the proposed array configuration (Fig. 12(c)), elements 2 and 3 are more dominant, forming an amplitude distribution indicative of tapering, which is a desirable characteristic for sidelobe suppression.

To quantitatively assess the impact of these amplitude distributions on sidelobe levels, Fig. 13 presents normalized array patterns derived using the method proposed in [30], with calculations performed in MATLAB. The proposed configuration clearly exhibits an amplitude tapering profile, yielding the lowest sidelobe levels among the compared configurations. In contrast, the array shown in Fig. 10(b) demonstrates the poorest sidelobe suppression performance due to its irregular amplitude distribution.

Beyond amplitude-based analysis, the current modeling framework also provides insights into the behavior of cross-polarization under beamforming scenarios. Fig. 14(a) and (b) show the relative phase shift ϕ applied to each array element during beam steering along the x-z and y-z planes, respectively. For elements that are inverted, the excitation phase is defined as $180° + \phi$. The modeling results indicate that the cross-polarization sources are effectively canceled due to the symmetric phase excitation of adjacent elements along the steering axis. This theoretical outcome suggests that if the array configuration is properly designed, the improvement in cross-polarization performance can be preserved even during dynamic beamforming—an assertion that will be experimentally verified in Section III.

Additionally, to verify that the antenna performance is preserved under beamforming scenarios, the active S-parameters were visualized as a scatter distribution chart, as shown in Fig. 15. A scan range from $-30°$ to $30°$ was evaluated, during which variations in impedance due to phase offsets were observed. Despite these variations, all configurations maintained values below -10 dB, indicating stable impedance matching across the scan angles. Here, in Fig. 15, the black circular scatter points denote the impedance of a representative antenna element within the array, extracted across the scan angle range. The surrounding box plots illustrate the interquartile range (IQR), encompassing the central 50% of the impedance values, thus providing insight into the variability and stability of the array's impedance performance under beam steering. These results, in conjunction with the theoretical analysis of cross-polarization behavior, confirm

(a)

(b)
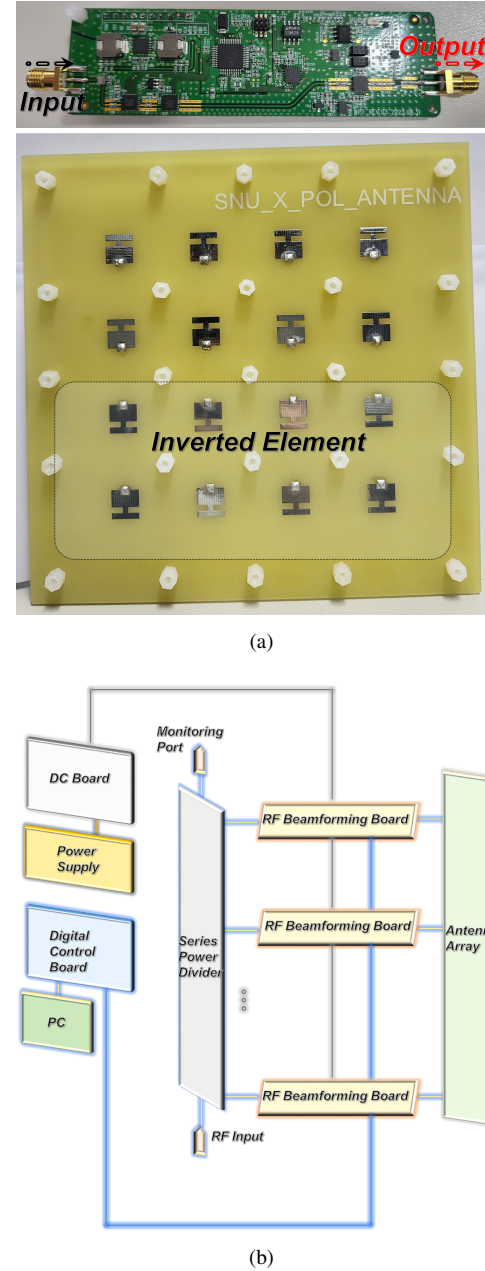
FIGURE 17. Photographs of fabricated hardware including (a) the beamforming board and antenna, and (b) the corresponding system-level block diagram.

the feasibility of effective beamforming with the proposed array configuration.

From a design standpoint, one of the key advantages of the proposed cross-polarization mitigation strategy lies in its integration into a structured design methodology, as outlined in Fig. 16. The process begins with selecting a suitable PCB substrate, factoring in considerations of cost and mechanical stability. Next, array layout and arrangement are determined, guided by insights from the cross-polarization modeling framework. The resulting radiation patterns are then evaluated in terms of gain, sidelobe levels, and cross-

FIGURE 18. Fabricated prototypes of (a) the series power divider and (b) the complete system including the measurement environment.

(a) (b)

FIGURE 19. Measurement results of the fabricated series power divider for each output port: (a) amplitude and (b) phase.
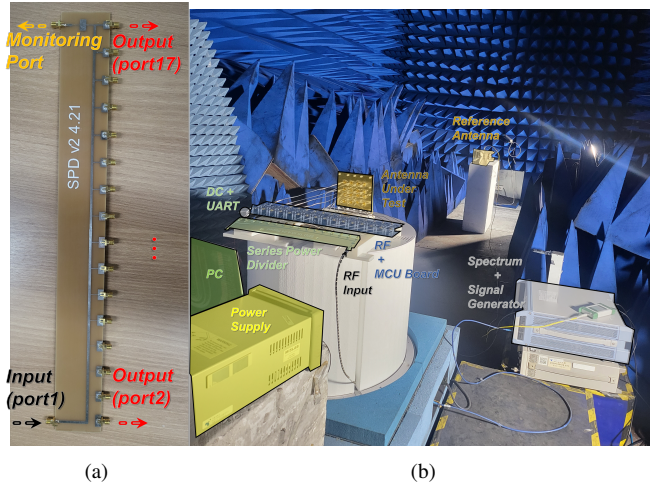

(a) (b)

FIGURE 20. Measured beam pattern of the proposed system at 5.8 GHz: (a) x-z plane and (b) y-z plane.

polarization performance, and benchmarked against results obtained from Floquet simulations. If deviations from the reference are observed, they are attributed to violations of the periodic structure assumed in Floquet analysis. To rectify this, the periodicity of the original and inverted elements is adjusted and restructured. This iterative approach enables the development of cross-polarization-optimized arrays through periodic reconfiguration, eliminating the need for a complete redesign of the antenna elements themselves. In summary, significant improvements in radiation performance can be realized simply by modifying the spatial arrangement of existing antennas within the array.

III. Measurement and Demonstration

Fig. 17(a) displays the fabricated beamforming board and antenna used for experimental validation. The beamforming board incorporates a 4-bit phase shifter capable of covering a full 360° range in 22.5° increments, with digital circuitry integrated to enable individual channel control. The antenna was constructed using two FR-4 substrates—one functioning as the radiator and the other as the ground plane—interconnected via coaxial connectors. To realize the air-substrate structure, nylon screws were employed as mechanical spacers. The overall system configuration is presented in Fig. 17(b), where power is supplied through an external source, and beamforming phases are controlled digitally via a microcontroller interface connected to a personal computer.

Prototypes of the proposed series power divider and the complete system, including the measurement setup, are shown in Fig. 18(a) and (b), respectively. All components were fabricated on FR-4 substrates in consideration of cost efficiency. Due to their one-dimensional growth in structure, series-type power dividers offer a more compact footprint compared to conventional parallel architectures, which scale in both dimensions relative to the number of outputs [31].
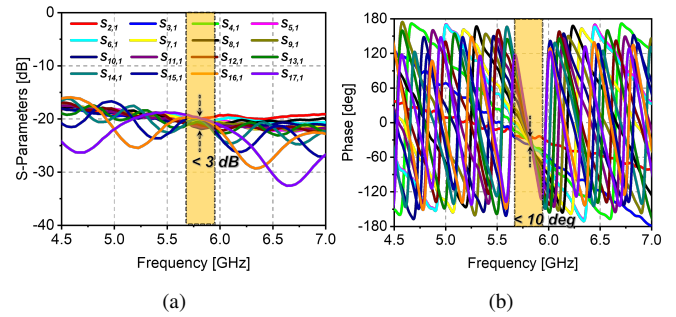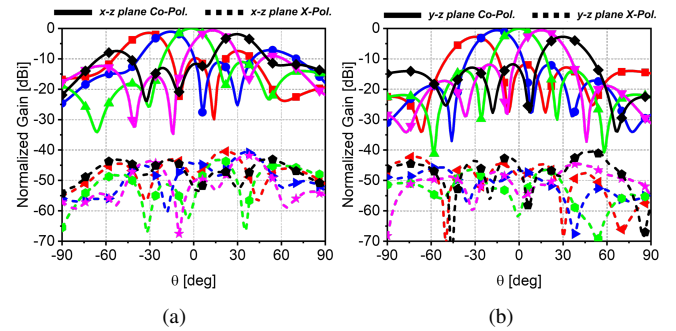
The amplitude and phase balance of the fabricated series power divider were measured, and the results are provided in Fig. 19(a) and (b). All 16 output ports exhibited amplitude variation within 3 dB and phase deviation within 10 degrees. Additionally, a dedicated monitoring port was implemented to facilitate input and output power verification.

This study presented a comprehensive analysis aimed at improving cross-polarization performance over the full angular range (θ) and under beam-steering conditions. To validate the proposed concept, a 16-channel beamforming system was developed, incorporating a microcontroller unit (MCU) to enable independent control of each channel. Communication with individual phase control modules is facilitated through a serial peripheral interface (SPI), while the MCU interfaces with a personal computer via the universal asynchronous receiver-transmitter (UART) protocol.

The measured beam patterns for the 4×4 antenna array are shown in Fig. 20(a) and (b), corresponding to the x-z and y-z planes, respectively, using the implemented 16-channel beam steering hardware. The experimental results exhibit strong agreement with the theoretical and simulated predictions discussed in previous sections. Notably, the measurements confirm that cross-polarization suppression is effectively maintained across all steering angles in both principal planes.

Table I presents a comparative evaluation of the proposed array configuration against state-of-the-art antenna systems. The analysis demonstrates that cross-polarization discrim-

TABLE 1. **Paper Comparison Table about Cross-Polarization Reduction Technique**

Ref.	Method	Array config.	XPD(dB)	SLL(dB)	Bandwidth(GHz)	Antenna Element Size(λ^3)	Scanning capability
[11]	Resonant frequency control	single	$\geq$-30	-	3.9-5 (24.6%)	1.4×0.46×0.06	no
[12]	Coupled $TM_{0,0.5}$ mode	single	$\geq$-30	-	1.65-1.68 (2 %)	0.14×0.22×0.22	no
[13]	A pair of open-ended stubs	single	$\geq$-21	-	2.6-2.65 (2 %)	0.22×0.41×0.02	no
[14]	Magnetic current reconstruction	single	$\geq$-20	-	1.88-1.9 (2 %)	0.1×0.15×0.02	no
[16]	Metal cylinders	1×8	$\geq$-35	12	2.35-2.45 (4 %)	0.35×0.44×0.06	yes
[18]	Suspended line	single	$\geq$-20	-	4.8-5.2 (8 %)	0.42×0.44×0.06	no
[19]	Array element rotating	8×8	$\geq$40	13	36-42 (15 %)	0.23×0.24*	yes
[20]	Array element rotating	8×8	$\geq$-35	13	26-32 (20 %)	0.24×0.25*	yes
[22]	Array element rotating	8×8	$\geq$-35	13	26-32 (20 %)	0.24×0.25*	yes
This work	Array element rotating	4×4	$\geq$-40	15	4.6-5.9 (24.7 %)	0.19×0.21×0.09	yes

* Not provided about the profile.

ination (XPD) benefits more significantly from array-level techniques than from element-level designs. Additionally, through structural selection and optimized arrangements, the proposed approach achieves notable advantages in sidelobe level (SLL) performance. The wide operational bandwidth was achieved by employing an indirect feeding mechanism and incorporating an air-substrate, with the fractional bandwidth calculated relative to the center frequency. Here, λ denotes the free-space wavelength ; the antenna element size refers exclusively to the dimensions of the radiator, excluding the ground plane.

IV. Conclusion

This paper proposes a comprehensive modeling framework for the analysis and mitigation of cross-polarization in TM_{10} mode patch antenna arrays. By introducing an equivalent electric current modeling approach, the study enables plane-specific evaluation of polarization behavior, offering a systematic basis for understanding and predicting the impact of various array configurations. Through this methodology, an optimized array layout was identified that effectively suppresses cross-polarization while preserving desirable characteristics such as low sidelobe levels and impedance matching performance. Unlike previous works that primarily achieved cross-polarization reduction through empirical array element rotation, the proposed modeling approach provides a physically grounded explanation for the formation and cancellation of cross-polarization components. It further extends this understanding to arbitrary array geometries, thus enabling a deeper physical understanding of how different array configurations influence cross-polarization behavior before engaging in detailed simulation processes. Additionally, by analyzing the impedance profiles and excited energy distributions of individual elements within the array, this work reveals the physical origins of sidelobe variations across different configurations, thus offering practical guidelines for array synthesis.

The proposed methodology was substantiated through both simulation and experimental validation. A compact beamforming system incorporating a series power divider
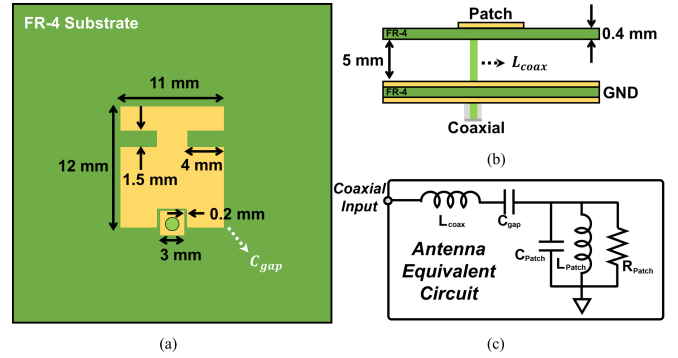

FIGURE 21. **The proposed antenna descriptions: (a) top view, (b) side view, and (c) equivalent circuit analysis.**

and a 16-channel phased array was fabricated and measured. The hardware implementation confirmed the feasibility of the proposed model, demonstrating consistent cross-polarization suppression across all beam-steering angles. Moreover, amplitude and phase imbalances were kept within 3 dB and 10 degrees, respectively, across all output ports, despite the miniaturized form factor of the power divider. Overall, this work provides a generalized and intuitive design methodology for polarization control in patch antenna arrays. The results indicate that significant cross-polarization suppression and sidelobe improvement can be achieved at the array level without any modification to the individual antenna element, thereby enhancing system-level design flexibility for advanced wireless communication applications.

V. Appendix
A. An Equivalent Circuit Analysis of the Antenna
In this paper, an air-substrate structure is implemented using two thin FR-4 substrates to enable wideband antenna design. The overall dimensions of the antenna are shown in Fig. 21(a) and (b). The two FR-4 substrates are supported by a nylon jig, which effectively creates an air-substrate environment. As a result, the antenna behaves as if it were constructed on a thick substrate, with the effective height
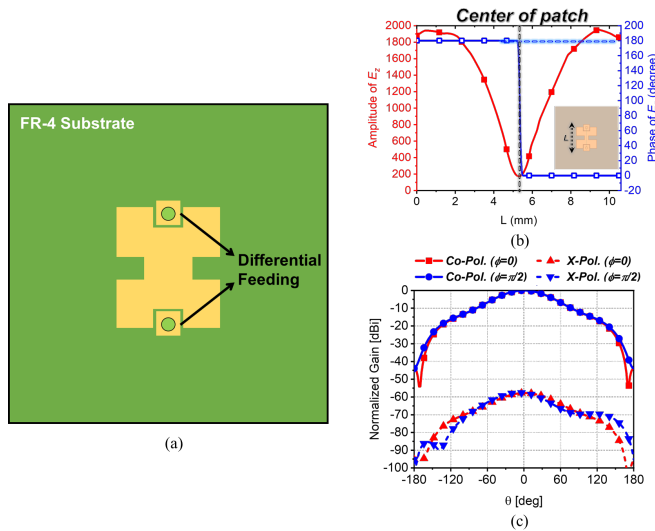
FIGURE 22. The differential antenna descriptions for cross-polarization analysis: (a) top view, (b) electric field result, and (c) beam pattern result.

determined by the nylon jig, thereby enabling wideband performance [32], [33].

However, directly connecting a coaxial feed to the patch introduces considerable inductance from the inner conductor passing through the thick substrate. To compensate for this effect, an indirect feeding method is adopted. As illustrated in Fig. 21(c), this approach goes beyond the conventional bandwidth enhancement attributed solely to the reduced Q-factor of a patch on a thick substrate. It strategically introduces a series resonance in the feeding network in combination with the inherent parallel resonance of the patch antenna, thereby enabling a significantly broader operational bandwidth.

B. Cross-Polarization Analysis of the Symmetric Antenna

To investigate the effect of electric current imbalance caused by asymmetric feeding, the proposed antenna structure in this paper was modified to adopt a differential feeding scheme, thereby achieving a fully symmetric configuration as shown in Fig. 22(a). The extracted electric field along the z-axis is presented in Fig. 22(b), which reveals a perfectly symmetric distribution, resembling the ideal TM_{10} mode, in contrast to the previously observed asymmetry.

As a result, the magnitudes of the electric currents at the non-radiating edges—responsible for cross-polarization—become exactly equal in amplitude and out-of-phase. This leads to effective cancellation across all planes and angles, as confirmed by the far-field beam pattern shown in Fig. 22(c), demonstrating significantly improved cross-polarization suppression.

REFERENCES

[1] J. S. Colburn, Y. Rahmat-Samii, M. A. Jensen, and G. J. Pottie, "Evaluation of personal communications dual-antenna handset diversity performance," *IEEE Trans. Veh. Technol.*, vol. 47, no. 3, pp. 737–746, 1998.

[2] Y. Li, Y.-X. Guo, and S. Xiao, "Orientation insensitive antenna with polarization diversity for wireless capsule endoscope system," *IEEE Trans. Antennas Propag.*, vol. 65, no. 7, pp. 3738–3743, 2017.

[3] B. Zhang, J. Ren, Y.-X. Sun, Y. Liu, and Y. Yin, "Four-port cylindrical pattern-and polarization-diversity dielectric resonator antenna for MIMO application," *IEEE Trans. Antennas Propag.*, vol. 70, no. 8, pp. 7136–7141, 2022.

[4] Z. Li, S. Wang, F. Li, L. Lin, and H. Zeng, "An I-shaped slot grid antenna array with substrate integration and enhanced bandwidth." *J. Electromagn. Eng. Sci.*, vol. 23, no. 5, 2023.

[5] S.-A. Lee, S.-J. Jo, S.-J. Kim, T.-K. Lee, and J. W. Lee, "Analysis of cross-polarized field by panel misalignment errors in a deployable reflector antenna," *J. Electromagn. Eng. Sci.*, vol. 23, no. 1, pp. 18–26, 2023.

[6] C. Andreu, S. Castelló-Palacios, C. Garcia-Pardo, A. Fornes-Leal, A. Vallés-Lluch, and N. Cardona, "Spatial in-body channel characterization using an accurate UWB phantom," *IEEE Trans. Microw. Theory Techn.*, vol. 64, no. 11, pp. 3995–4002, 2016.

[7] V. Kaim, B. K. Kanaujia, and K. Rambabu, "Quadrilateral spatial diversity circularly polarized MIMO cubic implantable antenna system for biotelemetry," *IEEE Trans. Antennas Propag.*, vol. 69, no. 3, pp. 1260–1272, 2020.

[8] J. Y. Sim and J.-R. Yang, "Frequency discrimination method using asymmetric transmission time in FSK radar," *J. Electromagn. Eng. Sci.*, vol. 22, no. 4, pp. 496–501, 2022.

[9] V. Kaim, N. Singh, B. K. Kanaujia, L. Matekovits, K. P. Esselle, and K. Rambabu, "Multi-channel implantable cubic rectenna MIMO system with cp diversity in orthogonal space for enhanced wireless power transfer in biotelemetry," *IEEE Trans. Antennas Propag.*, vol. 71, no. 1, pp. 200–214, 2022.

[10] H. Kim and J. Oh, "140-GHz wideband array antenna-in-package using multimode resonance," *IEEE Trans. Antennas Propag.*, vol. 71, no. 3, pp. 2136–2144, 2023.

[11] X. Zhang and L. Zhu, "Patch antennas with loading of a pair of shorting pins toward flexible impedance matching and low cross polarization," *IEEE Trans. Antennas Propag.*, vol. 64, no. 4, pp. 1226–1233, 2016.

[12] Z. Shao and Y. Zhang, "Cross-polarization reduction of shorted patch antenna by using coupled tm 0, 1/2 mode," *IEEE Trans. Antennas Propag.*, vol. 69, no. 12, pp. 8115–8124, 2021.

[13] N.-W. Liu, L. Zhu, Z.-X. Liu, Z.-Y. Zhang, G. Fu, and Y. Liu, "Cross-polarization reduction of a shorted patch antenna with broadside radiation using a pair of open-ended stubs," *IEEE Trans. Antennas Propag.*, vol. 68, no. 1, pp. 13–20, 2019.

[14] Z. Shao, Y. Hou, Y. Fang, and Y. Zhang, "Miniaturization and cross-polarization reduction of quarter-wave microstrip antennas based on magnetic currents reconstruction," *IEEE Trans. Magn.*, vol. 58, no. 11, pp. 1–6, 2022.

[15] N.-W. Liu, L. Zhu, G. Fu, and Y. Liu, "A low profile shorted-patch antenna with enhanced bandwidth and reduced H-plane cross-polarization," *IEEE Trans. Antennas Propag.*, vol. 66, no. 10, pp. 5602–5607, 2018.

[16] H. Chen and K.-L. Wu, "A cross-polarization suppressed probe-fed patch antenna and its applications to wide-angle beam-scanning arrays," *IEEE Trans. Antennas Propag.*, vol. 70, no. 9, pp. 7636–7645, 2022.

[17] Y. Luo, Q.-X. Chu, and D.-L. Wen, "A plus/minus 45 degree dual-polarized base-station antenna with enhanced cross-polarization discrimination via addition of four parasitic elements placed in a square contour," *IEEE Trans. Antennas Propag.*, vol. 64, no. 4, pp. 1514–1519, 2016.

[18] E. N. Moro, K. Ma, Y. Luo, N. Yan, and B. Tang, "H-plane cross-polarization reduction of a rectangular patch antenna using sisl technology," *IEEE Antennas Wireless Propag. Lett.*, vol. 20, no. 8, pp. 1532–1536, 2021.

[19] Y. Yin, S. Zihir, T. Kanar, Q. Ma, H. Chung, L. Gao, and G. M. Rebeiz, "A 37–42-GHz 8× 8 phased-array with 48–51-dbm EIRP, 64–QAM 30-Gb/s data rates, and EVM analysis versus channel RMS errors," *IEEE Trans. Microw. Theory Techn.*, vol. 68, no. 11, pp. 4753–4764, 2020.

[20] A. Nafe, M. Sayginer, K. Kibaroglu, and G. M. Rebeiz, "2x64 dual-polarized dual-beam single-aperture 28 GHz phased array with high cross-polarization rejection for 5G polarization MIMO," in *2019 IEEE*

MTT-S International Microwave Symposium (IMS). IEEE, 2019, pp. 484–487.

[21] H.-T. Hsu, A. Desai, Y.-F. Tsao, and H.-T. Chou, "Dual-band circularly-polarized antenna forming unit configurations featuring polarization selectivity and diversity for millimeter-wave satellite applications," *IEEE Trans. Veh. Technol.*, 2025.

[22] A. Nafe, M. Sayginer, K. Kibaroglu, and G. M. Rebeiz, "2×64-element dual-polarized dual-beam single-aperture 28-GHz phased array with 2×30 Gb/s links for 5G polarization MIMO," *IEEE Trans. Microw. Theory Techn.*, vol. 68, no. 9, pp. 3872–3884, 2020.

[23] T. Yoon and J. Oh, "Metal rods-based field concentrated common and differential modes theory enabling design of dual-polarized antennas," *IEEE Trans. Antennas Propag.*, 2023.

[24] V. G. Kasabegoudar and K. Vinoy, "Coplanar capacitively coupled probe fed microstrip antennas for wideband applications," *IEEE Trans. Antennas Propag.*, vol. 58, no. 10, pp. 3131–3138, 2010.

[25] T. Yoon, U. Park, and J. Oh, "Band-stop behavior vertically extended ground isolator based on transmission line theory for IBFD TRx decoupling applications," *IEEE Trans. Microw. Theory Techn.*, 2023.

[26] A. Lamminen, J. Säily, J. Ala-Laurinaho, J. de Cos, and V. Ermolov, "Patch antenna and antenna array on multilayer high-frequency pcb for d-band," *IEEE Open J. Antennas Propag.*, vol. 1, pp. 396–403, 2020.

[27] K. M. Mak, H. W. Lai, and K. M. Luk, "A 5G wideband patch antenna with antisymmetric L-shaped probe feeds," *IEEE Trans. Antennas Propag.*, vol. 66, no. 2, pp. 957–961, 2017.

[28] J. Guo, Y. Chen, D. Yang, K. Sun, J. Pan, and S. Liu, "Design of wideband filtering patch antenna array with high aperture efficiency and good filtering performance," *IEEE Trans. Antennas Propag.*, vol. 72, no. 1, pp. 974–979, 2023.

[29] S.-H. Wi, Y.-S. Lee, and J.-G. Yook, "Wideband microstrip patch antenna with U-shaped parasitic elements," *IEEE Trans. Antennas Propag.*, vol. 55, no. 4, pp. 1196–1199, 2007.

[30] J. Kim, W. Lee, and J. Oh, "Liquid-crystal-tuned resonant series patch array with unique element spacing emulating simplified operating construe of traveling-wave antenna," *IEEE Antennas Wireless Propag. Lett.*, 2023.

[31] D. Inserra and G. Wen, "Compact crossed dipole antenna with meandered series power divider for UHF RFID tag and handheld reader devices," *IEEE Trans. Antennas Propag.*, vol. 67, no. 6, pp. 4195–4199, 2019.

[32] D. M. Pozar, "Microstrip antennas," *Proc. IEEE*, vol. 80, no. 1, pp. 79–91, 2002.

[33] J. C. Zandboer, G. F. U. Johannsen, A. B. Smolders *et al.*, "A review on antenna technology developments for sub-THz wireless communication: Applications, challenges and opportunities," *IEEE Open J. Antennas Propag.*, 2025.

Taeyeong Yoon(Graduate Student Member, IEEE) received the B.S. degree (summa cum laude) in electronic engineering from Korea Aerospace University, Goyang, South Korea, in 2021, and the M.S. degree from the Department of Electrical and Computer Engineering, Seoul National University, Seoul, South Korea, in 2023, where he is currently pursuing the Ph.D. degree.

His current research interests include suppressing dual-polarized multi-path coupling, dual-polarized antennas for sub-6 GHz applications, high-efficiency power amplifiers for millimeter-wave (mm-wave) applications, and RF/mm-wave/microwave integrated circuits.

Uichan Park(Graduate Student Member, IEEE) received a B.S. degree in electronic and electrical engineering from Sungkyunkwan University, Suwon, South Korea, in 2020. He is currently pursuing an integrated master's and Ph.D. degree in the Department of Electrical and Computer engineering from Seoul National University, Seoul, South Korea. His current research interests include digital predistortion for RF power amplifiers, RF/mm-wave/microwave integrated circuits, and transmitarray antennas for 5G/6G communication systems.

Minje Kim(Graduate Student Member, IEEE) received a B.S. degree in electrical and computer engineering from Seoul National University, Seoul, South Korea, in 2023, where he is currently pursuing the integrated master's and Ph.D. degree. His current research interests include the diffusion model for EMI/EMC data generation and prediction, series power divider modeling, and the large-array wireless power transfer system.

Sanghun Lee(Graduate Student Member, IEEE) received the B.S. degree in electronic engineering from Kyungpook National University, South Korea, in 2014, and the M.S. degree from the Department of Electrical and Computer Engineering, Seoul National University, Seoul, South Korea, in 2025. His current research interests include microwave power transmission and RF Systems.

Since 2014, he has been with Samsung Electronics, Suwon, South Korea, as an RF circuit designer.

Young-Seok Lee(Graduate Student Member, IEEE) received a B.S. degree in the School of Electrical Engineering from Korea University, Seoul, South Korea, in 2021, and the M.S. degree from the Department of Electrical and Computer Engineering from Seoul National University, Seoul, South Korea, in 2023, where he is currently pursuing the Ph.D. degree.

His current research interests include wireless power transfer systems, optimization algorithms, and indoor localization.

Sangwook Nam(Senior Member, IEEE) received the B.S. degree from Seoul National University, Seoul, South Korea, in 1981, the M.S. degree from the Korea Advanced Institute of Science and Technology (KAIST), Daejeon, South Korea, in 1983, and the Ph.D. degree from The University of Texas at Austin, Austin, TX, USA, in 1989, all in electrical engineering.

From 1983 to 1986, he was a Post-Doctoral Researcher with the Gold Star Central Research Laboratory, Seoul. Since 1990, he has been a Professor with the School of Electrical Engineering and Computer Science, Seoul National University. His research interests include the analysis/design of electromagnetic structures, antennas, and microwave active/passive circuits.

Jungsuek Oh (Senior Member, IEEE) received his B.S. and M.S. degrees from Seoul National University, Korea, in 2002 and 2007, respectively, and a Ph.D. degree from the University of Michigan at Ann Arbor in 2012. From 2007 to 2008, he was with Korea Telecom as a hardware research engineer, working on the development of flexible RF devices. From 2013 to 2014, he was a staff RF engineer with Samsung Research America, Dallas, working as a project leader for the 5G/millimeter-wave antenna system. He is currently an Associate Professor in the School of Electrical and Computer Engineering, Seoul National University, South Korea. His research areas include mmWave beam focusing/shaping techniques, antenna miniaturization for integrated systems, and radio propagation modeling for indoor scenarios. He is the recipient of the 2011-2012 Rackham Predoctoral Fellowship Award, 2014 Samsung DMC R&D Innovation Award, 2018 SNU Creative Researcher Award, 2019 Samsung Electro-Mechanics Silver Prize, and the best paper awards from several conferences. He has published more than 60 technical journal and conference papers, and has served as a TPC member and as a session chair for the IEEE AP-S/USNC-URSI and ISAP. He has been a senior member of IEEE since 2017.